RSC Advances

ROYAL SOCIETY OF CHEMISTRY

www.rsc.org/advances

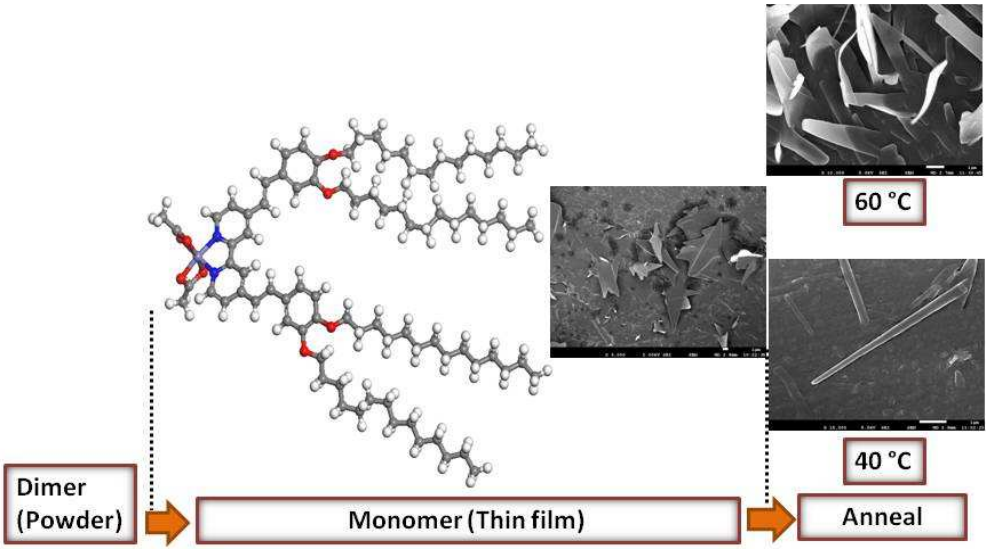

Monomeric, dimeric and polymeric iron(II) complexes of conjugated ligands exhibited differences in magnetic, mesomorphic and thermoelectric properties.

Journal Name

ARTICLE

Magnetic, thermal, mesomorphic and thermoelectric properties of mononuclear, dimeric and polymeric iron(II) complexes with conjugated ligands

Received 00th January 20xx,
Accepted 00th January 20xx

DOI: 10.1039/x0xx00000x

www.rsc.org/

Norbani Abdullah,[a] Mohamed Hamid Elsheikh,[b] Nik Muhd Jazli Nik Ibrahim,[a] Suhana Mohd Said,[c] Mohd Faizul Mohd Sabri,[b] Masjuki Haji Hassan[b] and Anita Marlina[a]

Three iron(II) complexes with conjugated multidonor ligands (L1 and L2) studied as thermally stable magnetic and thermoelectric materials were $[Fe_2(CH_3COO)_4(L1)_2]$ (**1**), $[Fe(L1)_3](BF_4)_2.4H_2O$ (**2**), and $\{[Fe_2(CH_3COO)_4(L2)].2H_2O\}_n$ (**3**). These complexes have low optical band gaps (1.9 eV for **1** and **2**, and 2.2 eV for **3**) and were magnetic with 57% high-spin Fe(II) in **1**, 33% in **2**, and 100% in **3** at 25 °C. Complex **1** melted at 57.2 °C and exhibited mesomorphism, while **2** melted at 96.9 °C, defining it as an ionic liquid. The thermal stabilities of **1** (T_{dec} = 199 °C) and **3** (T_{dec} = 191 °C) were lower than **2** (T_{dec} = 248 °C). Their Seebeck coefficients, S_e (in mV K^{-1}) were -0.65 for **1**, -0.54 for **2**, and +0.25 for **3**, identifying them as potential thermoelectric materials. Complex **1** formed stable thin films on quartz by the spin coating technique. The films formed at aging time t = 0 (F1) and t = 7 days (F2) were made up of monomers of **1**. The optical band gaps of the films (1.39 eV for F1 and 1.57 eV for F2) were lower than **1**. The films were free of cracks and have a fairly homogeneous morphology. The films with the best morphology were F1 annealed at 40 °C and F2 annealed at 60 °C.

Introduction

Complexes of first-row transition metal ions (valence electronic configuration d^4-d^7), with ligands of intermediate field strengths (mainly N-donors), have labile electronic configurations that may be reversibly switched from high spin (HS) to low spin (LS), or *vice versa*, when subjected to an external stimulus, such as temperature, pressure, light or magnetic field.[1-5] The properties of these complexes, such as colour and magnetism, depend on their spin states. Hence, these spin crossover (SCO) complexes are potential materials for memory storage and as thermochromic indicators and sensors.[6,7] However such applications require that the spin transition occurs abruptly at ambient temperature (ideally room temperature) and with wide thermal hysteresis (ΔT) for good memory effect. These characteristics require strong interactions between the SCO centres, which may occur through H-bonding, π-π[6,8] and/or covalent interactions (for multinuclear and polymeric compounds).[9] In the latter case, there may exist synergistic effects between SCO and magnetic exchange, particularly when it involves covalent bridges between the metal ions, and intra- and inter-cluster contributions. Kahn *et al*.[10] and Real[11] have postulated that extended networks of covalently bridged SCO centres should lead to enhanced cooperation and memory properties through efficient distribution of molecular distortions.

The most extensively studied SCO materials are complexes of iron(II) (d^6) with N-donor ligands.[5,12,13] More recently, these complexes were also studied as materials for dye-sensitised solar cells (DSSC)[14-20] and thermoelectrical applications.[21] Thermoelectricity involves the conversion of thermal energy directly to electrical energy. An important thermoelectrical parameter is the Seebeck coefficient (S_e), which can be determined from the slope of a linear graph of ΔV versus ΔT. This is based on the equation $\Delta V = S_e \Delta T$, where ΔV = potential difference and ΔT = temperature difference. The factors that determine the magnitude and sign of S_e are the entropy change and charge of the carrier, respectively. As examples, the S_e value (in mV K^{-1}) of $[Fe(CN)_6]^{3-/4-}$ was +1.4,[22] $[Co(bipy)_3]^{2+/3+}[Tf_2N]_{2/3}$ was +2.19,[21] and $[Co(L)_2]^{2+/3+}(BF_4)_{2/3}$ was +1.89.[23] The good thermoelectrical properties of these mixed-valence SCO complexes were ascribed to increased entropies of their cations (positive S_e values).

More recent research on SCO and DSSC materials now designs them to also have liquid-crystalline properties for the following reasons: facile formation of ordered thin films, enhancement of spin-transition signals, switching and sensing in different temperature regimes,[5,24] and directional electronic mobility.[25]

Our research group is focused on multifunctional molecular materials based on selected first-row transition metal complexes. This paper is an extension of our study on $[Fe_2(CH_3COO)_4(L1)_2]$ (**1**), where L1 was a π-conjugated N_2-donor ligand.[26] It reports the syntheses, structural deduction

[a] Department of Chemistry, Faculty of Science, University of Malaya, 50603 Kuala Lumpur.
[b] Department of Mechanical Engineering, University of Malaya, 50603 Kuala Lumpur, Malaysia.
[c] Department of Electrical Engineering, University of Malaya, 50603 Kuala Lumpur, Malaysia.

and magnetic properties of $[Fe(L1)_3](BF_4)_2.4H_2O$ (**2**) and $\{[Fe_2(CH_3COO)_4(L2)].2H_2O\}_n$ (**3**), where L2 was a conjugated N,S-donor ligand. This is followed by thermal, mesomorphic and thermoelectric properties of **1** – **3**. The structural formula of these materials are shown in **Fig. 1**. The objectives of this paper were to correlate nuclearity and bonding type of complexes with their physical properties. Finally, this paper reports the formation, characterization and surface morphology of thin films formed from **1** by the spin-coating technique under different aging time of its solutions and different annealing temperatures of the films.

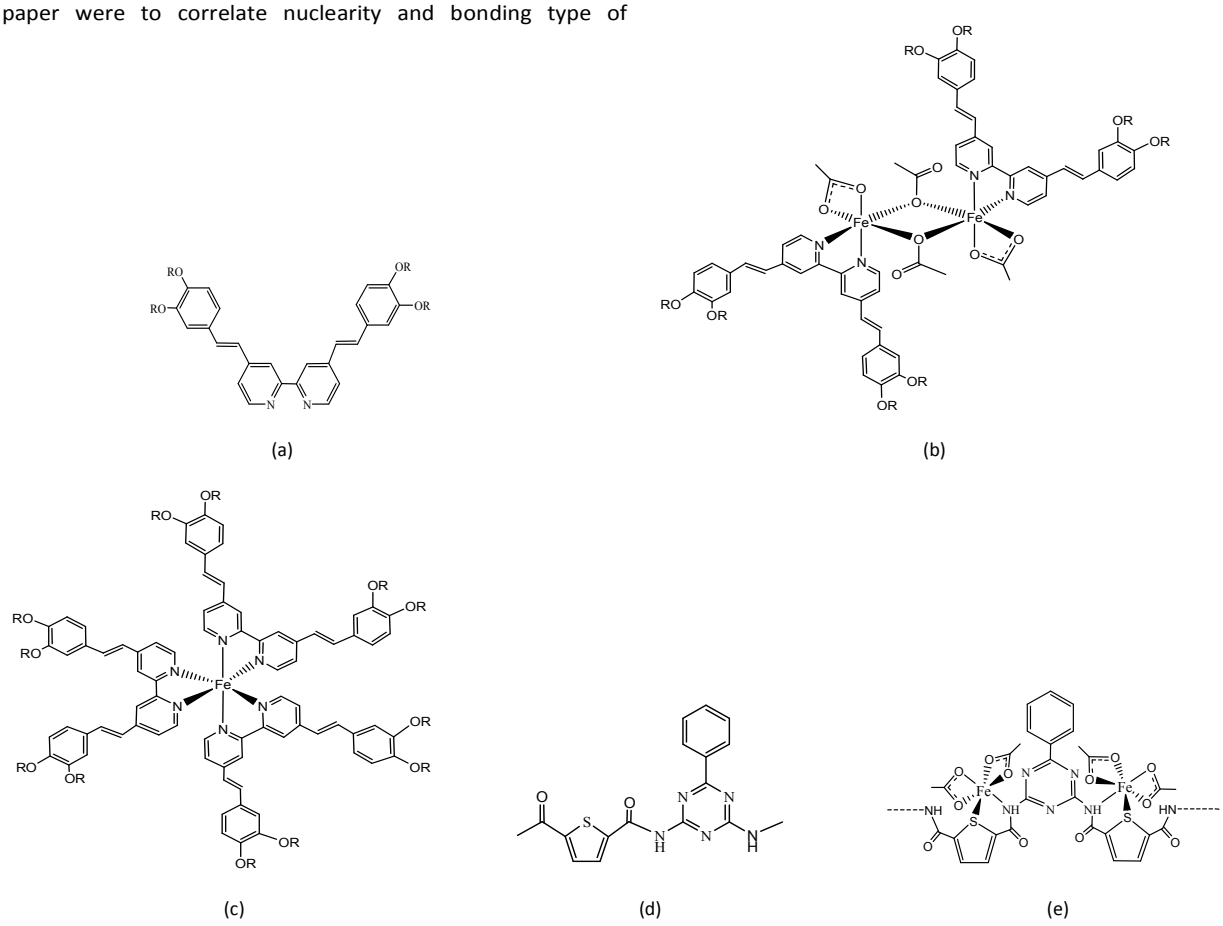

Fig. 1 Structural formulas of (a) L1[26], (b) **1**[26], (c) $\mathbf{2}^{2+}$, (d) L2 (a repeat unit), and (e) **3** (showing part of a polymeric structure); R = $CH_3(CH_2)_{13}$.

Experimental

General

Ligand L1 and complex **1** were synthesized and characterised as previously reported.[26] Other chemicals were commercially available and used as received.

Synthesis of $[Fe(L1)_3](BF_4)_2.4H_2O$ (2)

Iron(II) tetrafluoroborate hexahydrate (0.19 g, 0.57 mmol) and ascorbic acid (0.16 g, 0.91 mmol) were dissolved in methanol (50 cm^3) at room temperature, and N_2 was passed through the solution for about 15 min. A solution of L1 (2.0 g, 1.7 mmol) in chloroform was gradually added to the solution. The reaction mixture was stirred magnetically under N_2 at room temperature overnight. The solvents were removed on a rotary evaporator, and the dark purple powder formed was successively washed with distilled water, aqueous methanol (1:1 v/v), and methanol, and then dried in an oven at 60 °C. Yield: 1.58 g (72.0%). Anal. calcd. for $C_{246}H_{404}B_2F_8FeN_6O_{16}$: C, 75.16; H, 10.36; N, 2.14. Found: C, 75.06; H, 10.49; N, 2.21%.

Synthesis of L2

2,4-Diamino-6-phenyl-1,3,5-triazine (18.89 g, 100.9 mmol) was added portion wise to a solution of 2,5-thiophenedicarboxylic acid (12.93 g, 100.9 mmol) in absolute ethanol (100 cm^3). The mixture was refluxed for 2 h and then left to cool to room temperature. The white powder formed was filtered off, washed with ethanol and dried in an oven at 80 °C**.** Yield: 31.2 (97.9 %). ^{1}H-NMR (400 MHz, DMSO-d_6): δ = 8.23-8.25 (*d*, $2H_{aromatic}$), 7.71 (*s*, NH), 7.44-7.51 (*m*, $2H_{aromatic}$), 6.80 (*b*, $2H_{aromatic}$). Anal. calcd. for $C_{15}H_{11}N_5O_3S$: C, 52.8; H, 3.3; N, 20.5. Found: C, 52.6; H, 3.9; N, 20.7%.

Synthesis of $\{[Fe_2(CH_3COO)_4(L2)].2H_2O\}_n$ (3)

Iron(II) ethanoate (1.92 g, 11.0 mmol) was added to an ethanolic suspension of L2 (3.75 g, 11.0 mmol) and ascorbic acid (about 0.1 g). The mixture was heated under reflux for 3 h. The brown powder formed was filtered from the hot reaction mixture, washed with

ethanol, and dried in an oven at 100 °C. The yield was 4.98 g (87.8%). Anal. calcd. for the repeat unit $C_{23}H_{25}Fe_2N_5O_{12}S$: C, 39.3; H, 3.3; N, 9.9. Found: C, 39.1; H, 3.6; N, 9.7%.

Instruments

^{1}H-NMR spectrum was recorded on a JEOL FT-NMR lambda 400-MHz spectrometer. Elemental analyses were recorded on a Thermo Finnigan Flash EA 110 CHNS/O analyser. FTIR spectra were recorded from 4000 cm^{-1} to 450 cm^{-1} on a Perkin Elmer Frontier FTIR spectrophotometer equipped with a diamond attenuated total reflectance attachment. UV-vis spectra for solutions were recorded from 1200 to 400 nm on a Shimadzu UV-vis-NIR 3600 spectrophotometer, and for films from 1000 to 200 nm by using AvaSoft 8 software on a fibre optic AvaSpec-2048-USB2 spectrometer. Magnetic susceptibilities were measured on a Sherwood automagnetic susceptibility balance by the Gouy method, using $Hg[Co(NCS)_4]$ as the calibrant. A diamagnetic correction for each sample was estimated from Pascal's constants. Thermogravimetry (TG) was done on a Perkin Elmer Pyris Diamond TG/DTA thermal instrument under N_2 at a flow rate of 10 cm^3 min^{-1}. The temperature range was 50-900 °C, and the scan rate was 20 °C min^{-1}. Differential scanning calorimetry (DSC) was done on a Mettler Toledo DSC 822 calorimeter under N_2 at a flow rate of 20 cm^3 min^{-1}, and a scan rate of 10 °C min^{-1}. The onset temperatures were quoted for all peaks observed. The photomicrographs were captured on an Olympus polarizing microscope equipped with a Mettler Toledo FP90 central processor and a Linkam THMS 600 hot stage. The sample was finely ground and heated overnight in an oven at 60 °C to remove lattice water prior to analysis. The heating and cooling rates were 10 and 3 °C min^{-1} respectively, and the magnification was 50x. Thermoelectrical properties were measured for a solution (10 cm^3) made up of the complex (1.9 mM for **1**, 1.0 mM for **2**, and 1.0 mM for **3**), *tert*-butylammonium tetrafluoroborate (0.3 M) and KI-KI_3 (0.01 g). The solvent was $CHCl_3$ for **1** and **2**, and DMSO for **3**. The solution was filled into a cell made up of two compartments, each containing a platinum wire electrode precleaned with dilute HCl followed by distilled water. The compartments were placed in two separate water baths and connected by a salt bridge containing the same mixture. One water bath was heated with a hot plate (hot side) while the other was left at room temperature (cold side). The potential difference between the hot side and cold side was measured at 5 °C interval in the temperature range 25 to 55 °C using an Agilent 34461A Digital Multimeter. A controlled experiment was similarly done using a solution of KI-KI_3 (0.01 g) in $CHCl_3$ (10 cm^3).

Formation of thin films by the spin-coating technique

Two solutions of **1** (10.0%) in a mixture of chloroform and toluene (5:4 v/v) were prepared. The first solution was immediately spin-coated onto a quartz glass, while the second solution was kept in a sealed container for seven days before it was spin-coated onto the same substrate. The rate of rotation was 1000 rpm and the duration was 30 s. The resulting thin films (F1 and F2, respectively) were then annealed in air at 40 and 60 °C for 1 h.

Surface morphology of thin films

Atomic force microscopy (AFM) was done on a D-3000 Digital instruments, employing a contact mode cantilever tip model CONT10A from Bruker. All images were acquired in ambient air with the scan ranging from 0.5 to 1 Hz. The imaging time for each frame was between 5 to 10 min. The set point voltage was adjusted to the lowest possible voltage (between 1.6 and 2.5 V) to avoid damaging the films. Field emission scanning electron microscopy (FESEM) was done on a Jeol JSM-7600F. The magnifications were 3000x (F1 before annealing), 15000x (F1 at 40 °C), 10000x (F1 at 60 °C), and 10000x (for all F2 films). Elemental analyses were determined by energy dispersive X-ray electron spectroscopy (EDX).

Results and discussion

Syntheses and structural deductions

The ligand L1 was a N_2-donor with extended conjugated bonds and appended with four linear 14-carbon alkyloxy chains at the aromatic rings. It reacted with $[Fe(CH_3COO)_2]$ (mole ratio = 1:1) to form a dimeric neutral complex, $[Fe_2(CH_3COO)_4(L1)_2]$ (**1**),[26] and with $Fe(BF_4)_2.6H_2O$ (mole ratio = 3:1) to form a mononuclear ionic complex, $[Fe(L1)_3](BF_4)_2.4H_2O$ (**2**). On the other hand, the ligand L2 was a conjugated polymeric amide with N,S-donors. It reacted with $[Fe(CH_3COO)_2]$ (mole ratio = 1:1) to form a polymeric neutral complex, $\{[Fe_2(CH_3COO)_4(L2)].2H_2O\}_n$ (**3**). These complexes have octahedral Fe(II) atoms as shown in their proposed structural formulas (Fig. 1). The structure of **1** was reported previously,[26] while those of **2** and **3** were in accord with combined instrumental data (Table 1). The elemental analyses for C, H, and N (Experimental) for **2** and **3** were in good agreement with their chemical formulas.

Spectroscopic and magnetic studies

For these Fe(II) complexes, the IR spectra were mainly used to detect the presence of alkyloxy chain and to probe the binding mode of the carboxylate ion, while the UV-vis spectra were used to calculate the optical band gap (E_o) using the equation: $E_o = 1.24 \times 10^{-6}/\lambda$, where λ = absorption edge of the charge-transfer (CT) band in nm. The magnetic data ($\chi_M T$), obtained by the Gouy method at 25 °C, was to deduce the spin state, either low spin (LS) or high spin (HS), of Fe(II) atom.

For **2**, the IR spectrum showed two strong peaks at 2917 cm^{-1} ($\upsilon_{asym}CH_2$) and 2849 cm^{-1} ($\upsilon_{sym}CH_2$), respectively for the alkyloxy chains, and peaks at 1670 cm^{-1} for vinylic C=C, 1594 cm^{-1} for aromatic C=C, 1266 cm^{-1} for C-O, and 1054 cm^{-1} for BF_4^- ion. Its UV-vis spectrum, recorded in $CHCl_3$, showed two strong intraligand bands at 310 nm and 392 nm, and a strong singlet metal-to-ligand charge transfer (^{1}MLCT) band at 561 nm arising from LS Fe(II) atom. The E_o value was 1.9 eV, which was the same as **1**.[26] The $\chi_M T$ value was 1.0 cm^3 K mol^{-1}, indicating 33% HS and 67% LS Fe(II) atoms at 25 °C (since the expected value for a mononuclear HS Fe(II) complex is 3.01 cm^3 K mol^{-1},[1] while a LS Fe(II) complex is diamagnetic). The higher percentage of LS Fe(II) atom in **2** compared to **1** (Table 1) is consistent with a stronger ligand field (shorter Fe-N bonds) in the former complex (FeN_6 chromophore) compared to the latter (FeN_2O_4 chromophore).[26]

For **3**, the IR spectrum shows a medium peak for H_2O at 3316 cm^{-1}, a medium peak for C=O(amide) at 1637 cm^{-1}, a strong peak for $\upsilon_{asym}COO$ at 1522 cm^{-1}, a strong peak for $\upsilon_{sym}COO$ at 1394 cm^{-1}, and a medium peak for Fe-N bond at 595 cm^{-1}. Two important inferences from these data are: (a) the amide nitrogen was coordinated to Fe(II) since its value was shifted to

lower energy compared to L2 (1672 cm^{-1}), and (b) the CH_3COO^- ion was coordinated to Fe(II) as a chelating ligand since the value of Δ ($\upsilon_{asym}COO$ - $\upsilon_{sym}COO$) was 128 cm^{-1}.[28] The UV-vis spectrum, recorded in DMSO, showed two strong intraligand bands at 241 nm and 487 nm, and a weak *d-d* band at 831 nm assigned to $^5T_{2g} \rightarrow {}^5E_g$ transition for a HS Fe(II) atom.[17,24,27] The E_o value was 2.2 eV, which was larger than **1** and **2**, and could arise from the longer Fe-L2 bonds expected for HS Fe(II). Finally, the $\chi_M T$ value was 6.8 cm^3 K mol^{-1}, indicating 100% HS Fe(II).

Table 1 Spectroscopic, magnetic, thermogravimetric, and thermoelectric data for complexes **1** - **3**

Complex	IR Δ (cm^{-1})*	UV-vis λ_{max} (nm) ε_{max} (**)	E_o (eV)	Magnetic $\chi_M T$ (cm^3 K mol^{-1})	TG T_{dec} (°C)	Thermoelectric S_e (mV K^{-1})
$[Fe_2(CH_3COO)_4(L1)_2]$ (**1**)#	130 206	544 (0.2) 1412 (0.25) 1755 (0.25)	1.9	3.4 57% HS; 43% LS	199	-0.65
$[Fe(L1)_3](BF_4)_2.4H_2O$ (**2**)	-	310 (4.4) 392 (4.0) 561 (1.3)	1.9	1.0 33% HS; 67% LS	248	-0.54
$\{[Fe_2(CH_3COO)_4(L2)].2H_2O\}_n$ (**3**)	128	241 (1.3) 487 (0.36) 831 (0.02)	2.2	6.8 100% HS	191	+0.25

*Δ = $\upsilon_{asym}COO$ - $\upsilon_{sym}COO$ (from IR); **10^4 M^{-1} cm^{-1}; #spectral and magnetic data[26]

Thermal and mesomorphic properties

The thermal properties of **1**-**3** were studied by thermogravimetry (TG), while the mesomorphic properties of **1** and **2,** but not **3**, were studied by differential scanning calorimetry (DSC) and polarising optical microscopy (POM) since the former complexes were expected to exhibit mesomorphisms due to their anisotropic molecular shapes and the presence of long alkyloxy chains.[29]

For **1**, the TG trace shows a major mass loss of 97.0% (calc. 95.6%) from 199 to 612 °C due to the pyrolysis CH_3COO^- and L1 ligands. The DSC scans (**Fig. 2**) during the first cycle show two overlapping endothermic peaks (T_{range} = 57.2 – 74.2 °C; $\Delta H_{combined}$ = +127.6 kJ mol^{-1}) on heating, and a broad exothermic peak (T = 48.8 °C; ΔH = -189.9 kJ mol^{-1}) on cooling. These peaks were at almost the same T and ΔH values during the second cycle, indicating the reversibility of the phase transitions. However, the ΔH values for the overlapping endothermic peaks between the first and second heating cycles differ significantly. Under POM, the sample was observed to melt at about 60 °C to a very fluid dark red liquid. On cooling from 100 °C, a mixture of black and pale purple liquids formed at 67 °C. These liquids abruptly solidified at 60 °C to a mixture of orange-red and yellow solids, respectively. On further cooling to 30 °C, more of the orange-red solid changed to the yellow solid. On reheating, the orange-red solid changed its colour to purple, while the yellow solid formed fan-shaped textures at 70 °C (**Fig. 3**). On further heating, the colour of this texture changed to purple at 78 °C (Fig. 3). For comparison, the POM of L1, also recorded on cooling from its isotropic liquid phase (I_{iso} = 105 °C), shows needle-like textures at 83.8 °C which transformed to circular focal conic domains at 51.9 °C (**Fig. 3***).* However, the type of mesomorphisms for these compounds could not be ascertained in the absence of XRD data. Combining the DSC and POM results, and taking note that the colour of a LS Fe(II) is purple and a HS Fe(II) is white, thermal properties of **1** may be explained as follows: on heating, the dimeric complex melted at about 61.5 °C and cleared to I_{iso} at about 80 °C. On cooling from this temperature, it solidified at about 49 °C. From the colours observed on heating and cooling, it may be inferred that the complex exhibited a reverse SCO behavior in the temperature range 30 - 100 °C. Similar behavior was reported by Hayami *et al.* for $[Co(HO\text{-}C_{15}\text{-}terpy)_2](BF_4)_2$ in the temperature range -59 to -42 °C.[29] This behavior was ascribed to the fastening effect of the long alkyl chains. We are suggesting that the reverse SCO behavior noted for **1** arose from the weaker van der Waals interactions of the long alkyloxy chains of L1 bonded to the LS Fe(II) because of the less flexible geometry at this site (stronger Fe-L1 bond) compared to those bonded to the HS Fe(II). As a result, L1 at the HS site melted at a lower temperature, which enabled the Fe-L1 bonds to become shorter (stronger), causing a change in its electronic configuration to LS. These processes were reversed on cooling, but with a lower percentage of the LS Fe(II) (to account for the weaker endotherm observed from DSC during the second heating cycle).

For **2**, the TG trace showed a major mass loss of 94.5% (calc. 95.8%) from 248 to 744 °C due to the pyrolysis of BF_4^- ion and L1 ligand. The good agreement between the experimental and calculated values supports the proposed chemical formula. The DSC scans were recorded for two consecutive heating-cooling cycles in the temperature range 30 – 150 °C (**Fig. 2**). During the first cycle, there were two broad overlapping endothermic peaks (T_{range} = 87.0 – 105.0 °C; $\Delta H_{combined}$ = +84.2 kJ mol^{-1}) on heating, assigned to bond-breaking processes involving lattice H_2O and melting, and two corresponding exothermic peaks at T = 96.9 °C (ΔH = -63.1 kJ mol^{-1}) and 84.3 °C (ΔH = -7.6 kJ mol^{-1}) on cooling. These peaks were at almost the same T and ΔH values during the second cycle, indicating the reversibility of the phase transitions. Under POM, the sample was a dark red liquid at about 125 °C, but no optical textures were observed on cooling until it solidified at 96.5 °C. Hence, **2** may be regarded as an ionic liquid as it was an ionic compound with melting temperature lower than 100 °C.[30]

For **3**, the TG trace showed an initial mass loss of 5.1% (calc. 5.1%) at 75 °C, due to the evaporation of lattice H_2O, and a

major mass loss of 80.4% (calc. 79.1%) from 191 to 700 °C due to the pyrolysis of CH_3COO^- and L2 ligands. The good agreement between the experimental and calculated values supports the proposed chemical formula.

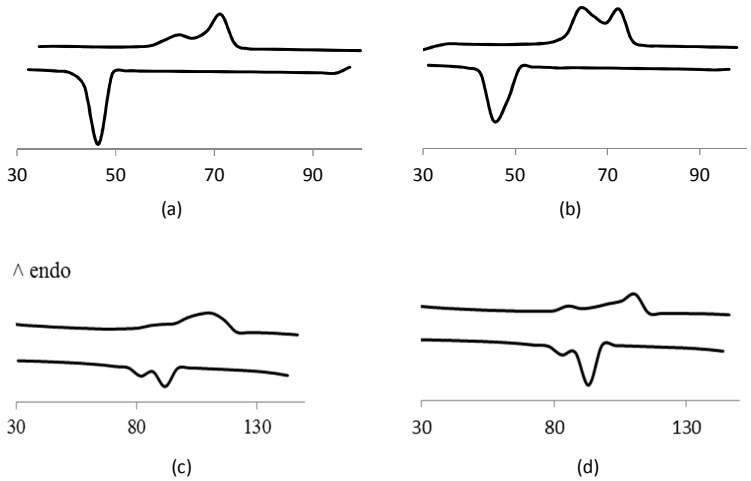

Fig. 2. DSC scans for: (a) **1** during first cycle (a) and second cycle (b); and **2** during first cycle (c) and second cycle (d). Heating (top), cooling (bottom).

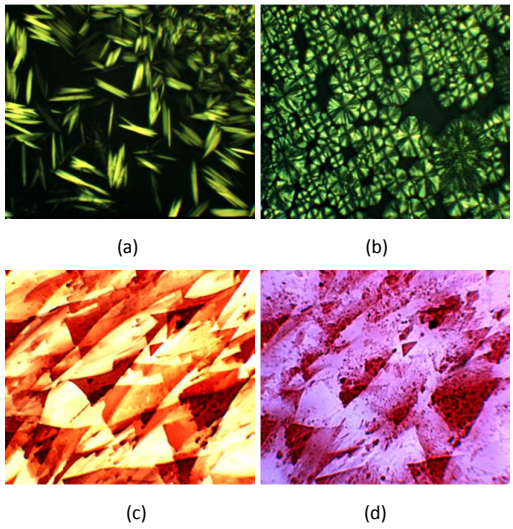

Fig. 3 Photomicrographs of: (a) L1 on cooling at 83.8 °C, (b) L1 on cooling at 51.9 °C, (c) **1** on heating at 70 °C and (d) **1** on heating at 78 °C.

Thermoelectric properties

SCO complexes of Fe(II) have the largest ΔS value (ΔS = 8.314 $\ln[(2S+1)_{HS}/(2S+1)_{LS}]$ = 13.38 J K^{-1} mol^{-1}) for the electronic transition from LS (S = 0) to HS (S = 2) when compared to SCO complexes of other metal(II) ions. Accordingly, these complexes are expected to have good thermoelectric properties. We present preliminary thermoelectric studies of complexes **1** – **3** by determining their Seebeck coefficients. The graphs of ΔV versus ΔT for these complexes (Fig. 4) were almost linear, with negative slopes for **1** and **2**, and a positive slope for **3**. The S_e value (mV K^{-1}), calculated as average of six readings from three heating-and-cooling cycles, was -0.65 ± 0.02 for **1**, -0.54 ± 0.02 for **2**, and +0.25 ± 0.05 for **3**. A control experiment done for a solution of KI-KI_3 in $CHCl_3$ gave S_e = -0.03 mV K^{-1}.

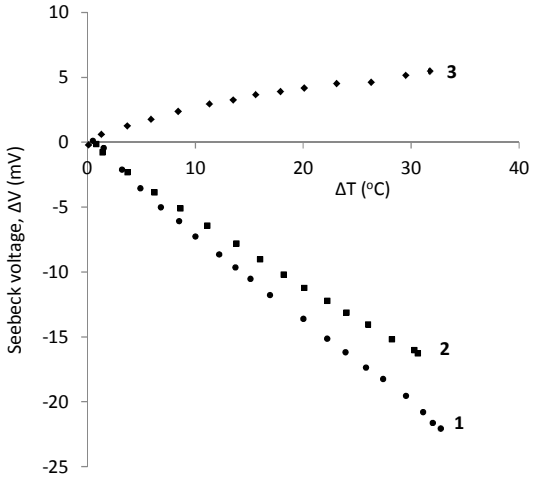

Fig. 4 Plots of ΔV versus ΔT for **1 – 3**.

The sign of S_e is thought to be dominated by ions with smaller mass and volume as these correlate to a higher mobility during the ionic conduction process. Accordingly for **1** and **2**, the negative S_e values were due to CH_3COO^- and BF_4^- anions, respectively, which are more mobile than the larger and sterically demanding cationic complexes. This is known as the Soret effect. Conversely for **3,** the ionic conduction was dominated by Fe(II) cation. It is proposed that, due to the weak Fe-L2 bonds, this complex dissociated to CH_3COO^- ion, Fe(II) ion, and neutral polymeric ligand (L2) in DMSO. Under the

influence of a potential difference, the CH_3COO^- ion and Fe(II) ion moved in the opposite direction. However, since Fe(II) ion is smaller and carries a higher charge compared to CH_3COO^- ion, it is expected to move faster, resulting in an overall positive S_e. It is noted that the magnitude of S_e values were comparable to the mixed-valence complexes reported in the literature.[21,22,31] Hence, these monovalence complexes are promising thermoelectric materials.

Formation of thin films from 1

Based on previous[26] and current findings, complex **1** was most promising as a DSSC, SCO and thermoelectric material compared to **2** and **3**. Hence, we proceeded to form thin films of this complex by the spin coating technique. Stable thin films were formed when the complex was dissolved in a mixture of chloroform and toluene (5:4 v/v) under two different conditions: (a) from freshly prepared solution (labelled F1), and (b) after the solution was kept at room temperature for 7 days (labelled F2). The films were then annealed at 40 °C and 60 °C (lower than the melting temperature of **1**). The thicknesses of the film, measured using a surface profiler, were in the range of 1.2 µm to 1.4 µm.

Structural studies of thin films by FTIR spectroscopy

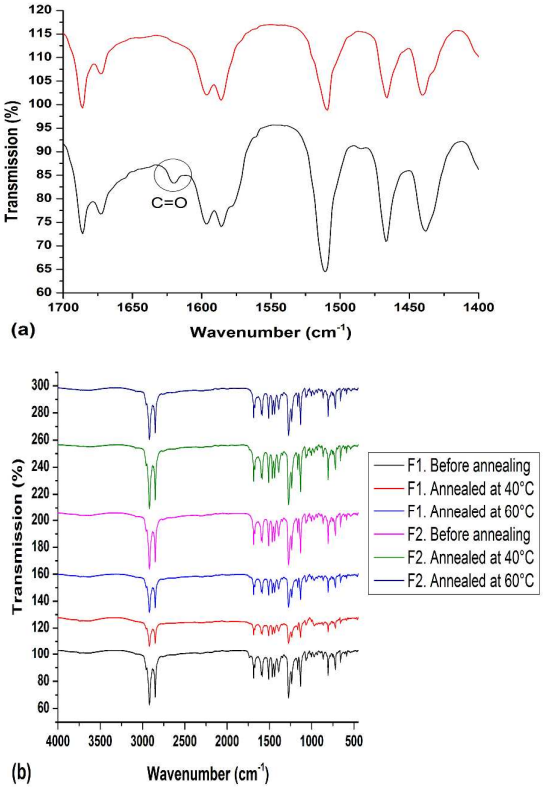

Fig. 5 FTIR spectra of: (a) **1** (black) and F1 annealed at 60 °C (red); and (b) F1 and F2 before and after annealing at 40 °C and 60 °C.

FTIR spectroscopy was used to compare the structure of **1** before and after the formation of thin films. We noted from **Fig. 5**(**a**) that the peak at 1620 cm^{-1} found in the spectrum of **1** and assigned to C=O of the monodentate bridging CH_3COO^- ligand, was absent in the spectrum of F1. From this, it may be inferred that the binding mode of this ligand changed to chelating when the dimers in the solid dissociated to monomers in solution, as shown in the following equation:

$$[Fe_2(CH_3COO)_4(L1)_2] \rightarrow 2\,[Fe(CH_3COO)_2(L1)]$$

We also noted similar FTIR spectra of these films at different annealing temperatures (**Fig. 5**), indicating minimal thermal effect on the structure of the complex in this temperature range

SCO behaviour and bandgaps of thin films

The UV-Vis spectra of these films (**Fig. 6**) show a strong ^{1}MLCT peak for LS Fe(II) at 550 nm, which was similar to **1** (544 nm[26]). However, the intensity of the ^{1}MLCT band in the films increased with increasing annealing temperatures (**Fig. 6**). From this, we infer that the monomers in the films showed similar reverse SCO behaviour as **1** on heating from room temperature to 60 °C. Finally, the band gaps (E_g) were 1.57 eV for F1 and 1.39 eV for F2. These values were lower than found for **1** (1.9 eV).[26] Hence, thin films formed from this complex maybe used in DSSC.

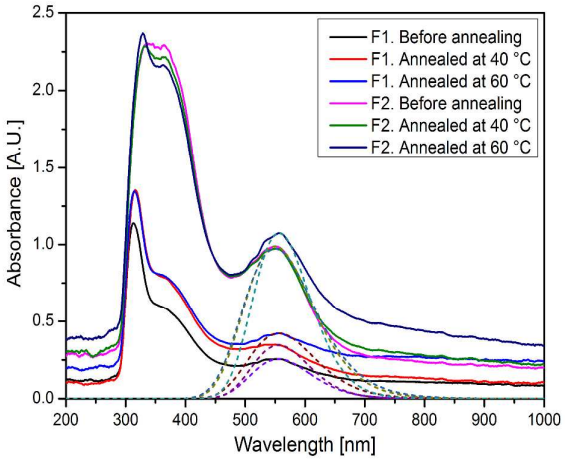

Fig. 6 UV-vis spectra of F1 and F2 (the deconvoluted spectra are shown by dashed lines).

Surface morphologies of films by AFM and FESEM

Images for the thin films by atomic force microscopy (AFM) are shown in **Fig. 7**. From these images, the root mean square roughness (RMS), height roughness (R_a) and grain mean size (*s*) were determined (Table 2).

Firstly, both F1 and F2 have almost similar values for RMS, R_a and *s* before annealing. However for F1, the values before annealing were significantly higher than after it was annealed at 40 °C, but lower than when it was annealed at 60 °C. The effect of annealing temperatures seems to be the opposite for F2 (higher at 40 °C than at 60 °C).

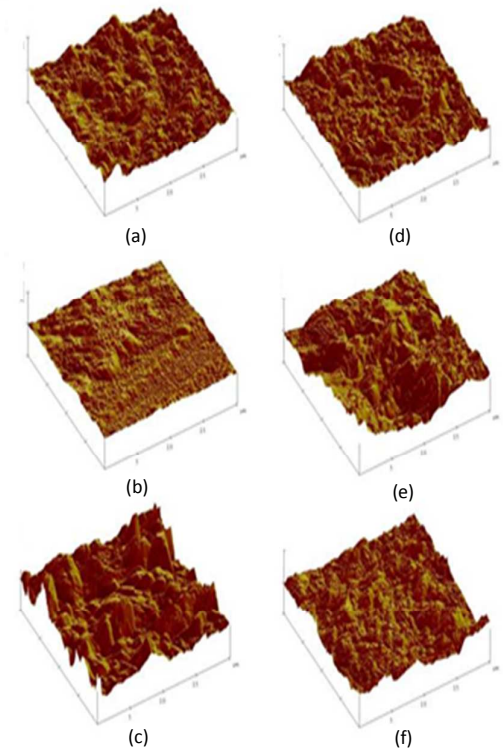

Fig. 7 AFM of F1: (a) before annealing, (b) annealed at 40 °C, and (c) annealed at 60 °C; and F2 (d) before annealing, (e) annealed at 40 °C, and (f) annealed at 60 °C.

Table 2 Root mean square roughness (RMS), height roughness (R_a) and grain mean size (*s*) for F1 and F2 at different annealing temperature (T)

Film	T (°C)	RMS (nm)	R_a (nm)	*s* (μm^2)
F1	-	68.8	54.3	2.70
	40	42.3	35.7	1.39
	60	97.3	80.6	5.91
F2	-	72.8	54.8	3.16
	40	124.5	100.0	3.12
	60	70.9	54.7	1.84

In order to understand the peculiarities found from AFM, we recorded the FESEM images of these films, and pasted at the bottom right-hand corner of each image, the colour of each film captured under a microscope.

F1 was the film formed from freshly prepared solution of **1**. Its colour was initially white, indicating that the mononuclear complex has mainly HS Fe(II) atoms. It is proposed that immediately after the dimeric molecules of **1** dissociated, most of the mononuclear complex molecules formed have long Fe-N and Fe-O bonds. Consequently, the molecules deposited as thin films on the quartz surface have mainly HS Fe(II) atom. Its FESEM images (**Fig. 8**) show sheet-like structures (length about 5-9 µm) before annealing, nanorod structures (length about 7 µm; width about 300 nm) after annealing at 40°C, and ribbon structures (length about 8 µm; width about 800 nm) after annealing at 60 °C. The observed changes were accompanied by the appearance of regions of purple color of LS Fe(II) in the film, which became darker and more uniform at 60 °C. From these observations, we infer that: (a) the Fe(II) atom in the complex changed from HS to LS on heating, indicating reverse SCO behaviour as similarly observed for **1**; (b) both HS and LS Fe(II) have similar lengths; and (c) HS Fe(II) complex has a smaller diameter than LS Fe(II) complex.

On the other hand, F2 was the film formed after a solution of **1** was left to age for a week at room temperature. Its colour was dark purple before and after annealing at 40 °C and 60 °C, indicating that the mononuclear complex has mainly LS Fe(II) atoms in this temperature range. This suggests that when the solution was left to age for a week, a more stable mononuclear complex was formed (shorter Fe-N and Fe-O bonds). Consequently, the molecules deposited have mainly LS Fe(II) atoms. Its FESEM images (**Fig. 8**) show cylindrical nanorod structures (length about 8-10 µm; width about 500 nm) before annealing, ribbon structures (length about 8-10 µm; width about 500-800 nm) after annealing at 40 °C, and wider ribbon structures (about 800-1000 nm) after annealing at 60 °C. Hence, the width of LS Fe(II) complex increased with temperature.

Finally, chemical element mapping were performed using the energy dispersive X-ray electron spectroscopy (EDX) to establish the chemical composition of these thin films. The results are shown in **Fig. 9**. The elements detected were Mg, Si, Na and Ca from the quartz substrate. This indicates a possible detection of the substrate surface through the small pores of the films. The results also showed a high content of carbon, which gives excellent agreement with the CHN elemental analyses for **1** (C, 74.96%[26]). It is also important to note that line EDX analysis in different samples shows chemical homogeneity of the films.

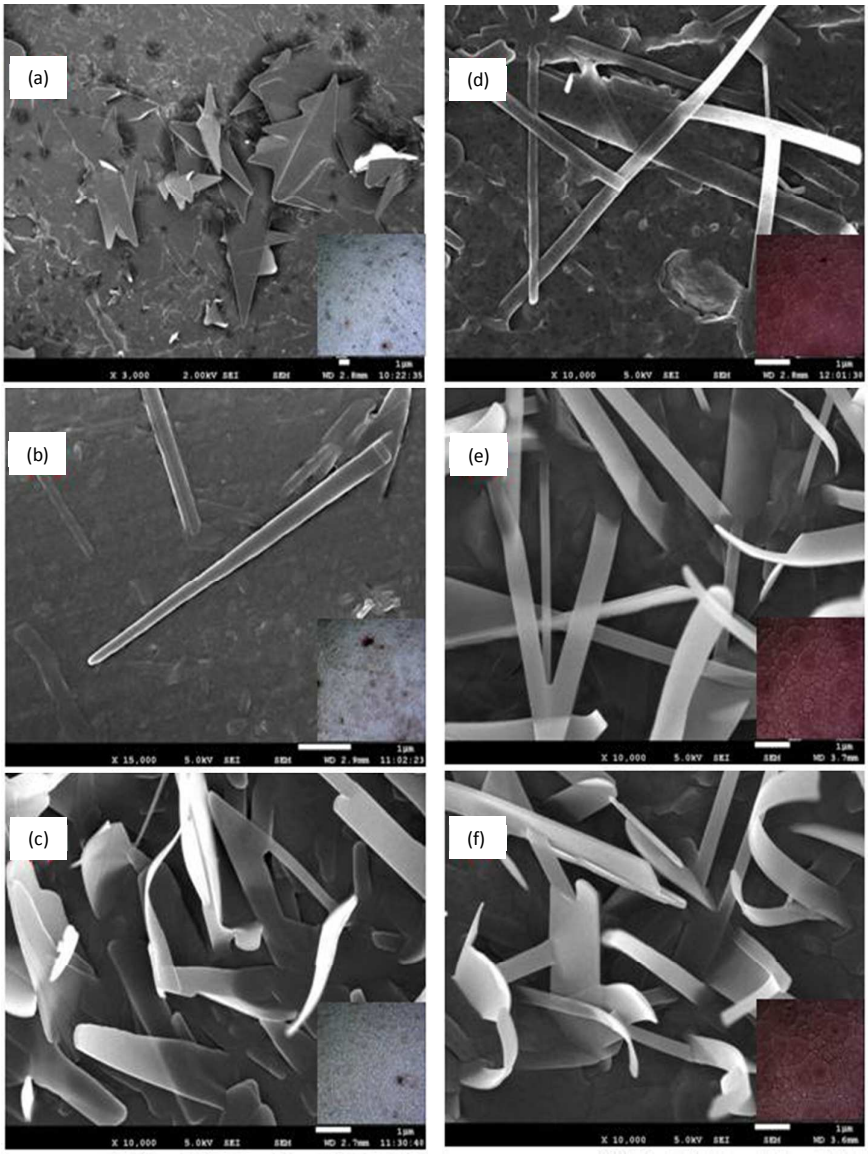

Fig. 8 FESEM images of: F1before annealing (a), annealed at 40 °C (b), and annealed at 60 °C (c); F2 before annealing (d), annealed at 40 °C (e), and annealed at 60 °C (f).

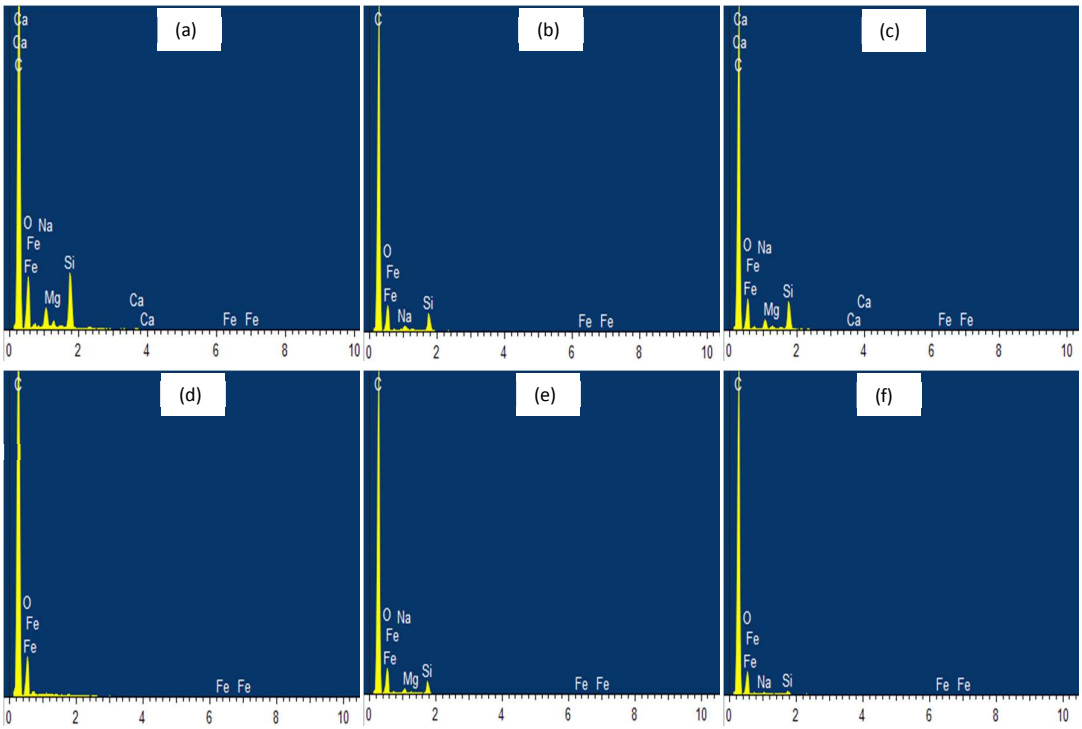

Fig. 9 EDX analyses for the surface of F1 before annealing (a), annealed at 40 °C (b), and annealed at 60 °C (c); and F2 before annealing (d), annealed at 40 °C (e), and annealed at 60 °C (f).

Conclusions

Three Fe(II) complexes reported in this paper were ($[Fe_2(CH_3COO)_4(L1)_2]$) (**1**), $[Fe(L1)_3](BF_4)_2.4H_2O$ (**2**) and $\{[Fe_2(CH_3COO)_4(L2].2H_2O)\}_n$ (**3**), where L1 and L2 were conjugated N_2-donor and N,S-donor ligands, respectively. These complexes have low optical bandgaps (1.9 eV for **1** and **2**, and 2.2 eV for **3**) and were magnetic with 57% HS Fe(II) in **1**, 33% HS Fe(II) in **2**, and 100% HS Fe(II) in **3** at 25 ^oC. The mixed spin states for **1** and **2** were consistent with the moderate field effect of FeN_2O_4 and FeN_6 chromophores, respectively, while the HS state for **3** was consistent with the weak field effect of $FeNO_4S$ chromophore. In addition, **1** exhibited reverse SCO behavior. The thermal stabilities of these complexes were in the following order: **1** ≈ **3** < **2**, and were initiated by pyrolisis of CH_3COO^- ligand. Both **1** and **2** melted at temperatures lower than 100 ^oC. Complex **1** was a liquid crystal, while **2** was an ionic liquid. Complexes **1** and **2** have negative S_e values (-0.65 mV K^{-1} for **1** and -0.54 mV K^{-1} for **2**), while **3** has a positive S_e value (+0.25 mV K^{-1}). Complex **1** formed stable thin films, F1 (t = 0) and F2 (t = 7 days), on quartz by the spin coating technique. The films were made up of monomers of **1**, and have lower bandgaps but similar reverse SCO behaviour compared to its dimers. The HS complex in F1 have sheet-like structure before annealing which changed to cylindrical nanorods and nanoribbons after annealing, while the LS complex in F2 have nanorod structure before annealing which changed to nanoribbons after annealing. All films showed a typical film microstructure, free of cracks and a fairly homogeneous morphology. However, F1 annealed at 40 ^oC and F2 annealed at 60 ^oC have the best film morphology in terms of lowest surface roughness and smallest grain size.

Acknowledgements

The authors thank Malaysia Ministry of Education for High Impact Research Grants (UM.C/625/1/HIR/MOHE/05 and UM.C/625/1/HIR/MOHE/ENG/29) and University of Malaya for research grants (RP014A-13AET, PV056-2012A and PG114-2014B).

References

1 O. Kahn, *Molecular Magnetism*. VCH Publishers Inc.: New York, 1993.
2 P. Gütlich, H. A. Goodwin, Eds. *Spin Crossover in Transition Metal Compounds*. Topics in Current Chemistry. Springer, Berlin-Heidelberg, 2004, 233.
3 C. Atmani, F. E. Hajj. S. Benmansour, M. Marchivie, S. Triki, F. Conan, V. Patinec, H. Handel, G. Dupouy and C. J. Gómez-García, *Coord. Chem. Rev*., 2010, **254**, 1559.
4 A. B. Gaspar, M. Seredyuk, P. Gütlich, *J. Mol. Struct*., 2009, **924-926**, 9.
5 Y. Bodenthin, G. Schwarz, Z. Tomkowicz, M. Lommel, Th. Geue, W. Haase, H. Möhwald, U. Pietsch and D. G. Kurth, *Coord. Chem. Rev*., 2009, **253**, 2414.
6 P. Gütlich, Y. Garcia and H. A. Goodwin, *Chem. Soc. Rev*., 2000, **29**, 419.
7 O. Kahn, *Nature*, 1999, **399**, 21.
8 P. Gütlich, *Struct. Bond*., 1981, **44**, 83.

9 G. Dupouy, M. Marchivie, S. Triki, J. Sala-Pala, C. J. Gomez-Garcıa, S. Pillet, C. Lecomtec and J. F. Letard, *Chem. Comm*., 2009, 3404.
10 O. Kahn, E. Codjovi, Y. Garcia, P. J. van Koningsbruggen, R. Lapouyade and L. Sommier, *ACS Symp. Ser*., 1996, **644**, 298.
11 J. A. Real, *Bistability in Iron(II) Spin-crossover Systems*. In: Sauvage JP (eds) Transition Metals in Supramolecular Chemistry. Wiley, New York, 1999, 51.
12 R. J. Wei, J. Tao, R. B. Huang and L. S. Zheng, *Eur. J. Inorg. Chem*., 2013, 916.
13 S. Heider, H. Petzold and G. Teucher, *Eur. J. Inorg. Chem*., 2013, 2382.
14 S. Ferrere and B. A. Gregg, *J. Am. Chem. Soc*., 1998, **120**, 843.
15 S. Ferrere, *Chem. Mater*., 2000, **12**, 1083.
16 S. Ferrere, *Inorg. Chim. Acta*, 2002, **329**, 79.
17 A. Hagfeldt and M. Grätzel, *Acc. Chem. Res*., 2000, **33**, 269-277.
18 S. Günes and N. S. Sariciftci, *Inorg. Chim. Acta*, 2008, **361**, 581.
19 N. Sekar and V. Y. Gehlot , *Resonance*, 2010, **15**, 819.
20 A. Hagfeldt, G. Boschloo, L. Sun, L. Kloo and H. Pettersson, *Chem. Rev*., 2010, **110**, 6595.
21 T. J. Abraham, D. R. MacFarlane and J. M. Pringle, *Energy Environ. Sci.,* 2013, **6**, 2639.
22 T. J. Kang, S. Fang, M. E. Kozlov, C. S. Haines, N. Li, Y. H. Kim, Y. Chen and R. H. Baughman, *Adv. Funct. Mater.,* 2012, **22**, 477.
23 N. Abdullah, N. L. M. Noor, A. R. Nordin, M. A. Halcrow, D. R. MacFarlane, M. A. Lazar, J. M. Pringle, D. W. Bruce, B. Donnio and B Heinrich, *J. Mater. Chem. C*, 2015, **3**, 2491.
24 P. G Bomben, K. C. D. Robson, B. D. Koivisto and C. P. Berlinguette, *Coord. Chem. Rev*., 2012, **256**, 1438.
25 R. M. O'Donnell, P. G. Johansson, M. Abrahamsson and G. J. Meyer, *Inorg. Chem*., 2013, **52**, 6839.
26 N. Abdullah, S. M. Said, A. Marlina, M. F. Roslan, A. Azil and A. R. Nordin, *The Sci World J*., 2015 (http://dx.doi.org/10.1155/2015/860537)
27 M. B. Bushueva, V. P. Krivopalov, E. B. Nikolaenkova, V. A. Daletsky, G. A. Berezovskii, L. A. Sheludyakova and V. A. Varnek, *Polyhedron*, 2012, **43**, 81.
28 G. B. Deacon and R. J. Philips, *Coord. Chem. Rev*., 1980, **33**, 227.
29 Y. Komatsu, K. Kato, Y. Yamamoto, H. Kamihata, Y. H. Lee, A. Fuyuhiro, S. Kawata and S. Hayami, *Eur. J. Inorg. Chem*., 2012, 2769.
30 M. F. R. Moita, M. L. T. S. Duarte and R. J. Fausto, *J. Chem. Soc. Faraday Trans*., 1994, **9**, 2953.
31 B. Burrows, *J. Electrochem. Soc*., 1976, **123**, 154.

Figures

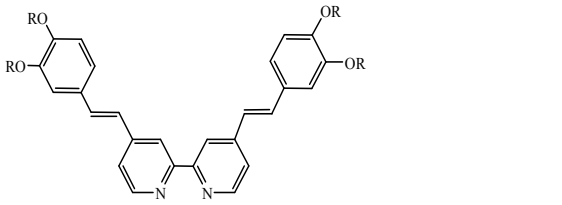

(a)

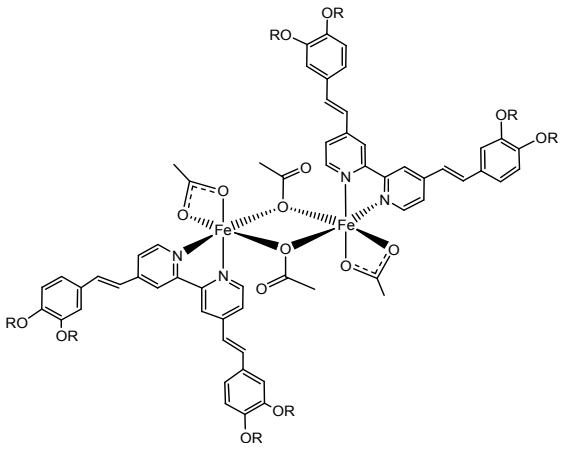

(b)

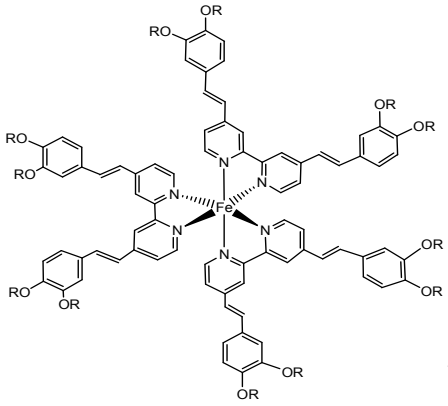

(c)

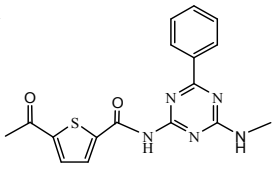

(d)

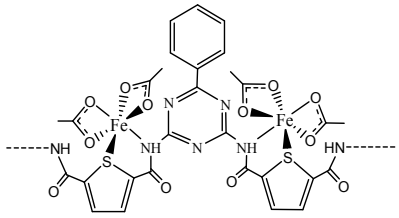

(e)

Fig. 1 Structural formulas of (a) L1[26], (b) **1**[26], (c) **2**$^{2+}$, (d) L2 (a repeat unit), and (e) **3** (showing part of a polymeric structure); R = $CH_3(CH_2)_{13}$.

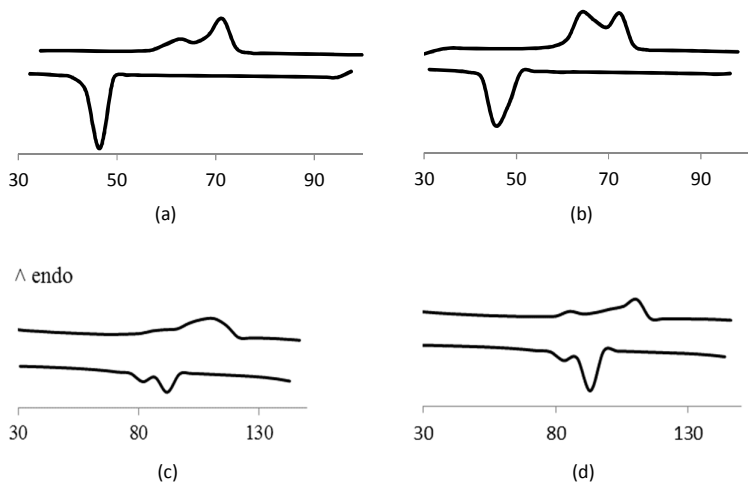

Fig. 2. DSC scans for: (a) **1** during first cycle (a) and second cycle (b); and **2** during first cycle (c) and second cycle (d). Heating (top), cooling (bottom).

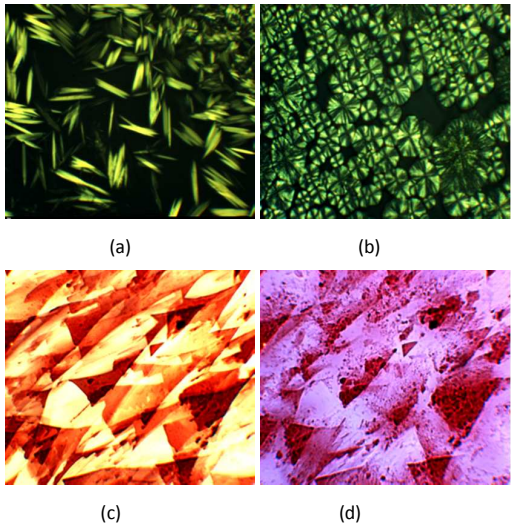

(a) (b)

(c) (d)

Fig. 3 Photomicrographs of: (a) L1 on cooling at 83.8 °C, (b) L1 on cooling at 51.9 °C, (c) **1** on heating at 70 °C and (d) **1** on heating at 78 °C.

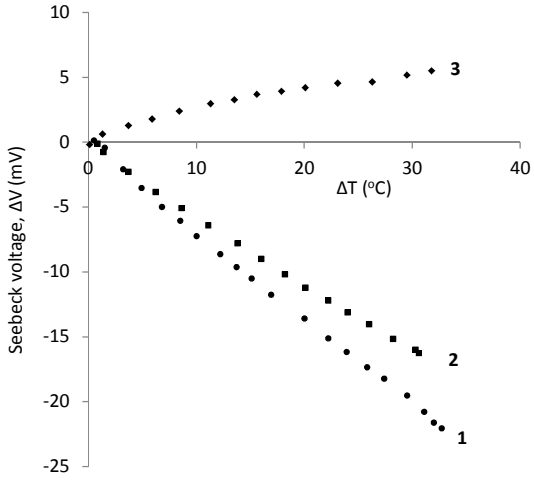

Fig. 4 Plots of ΔV versus ΔT for **1 – 3**.

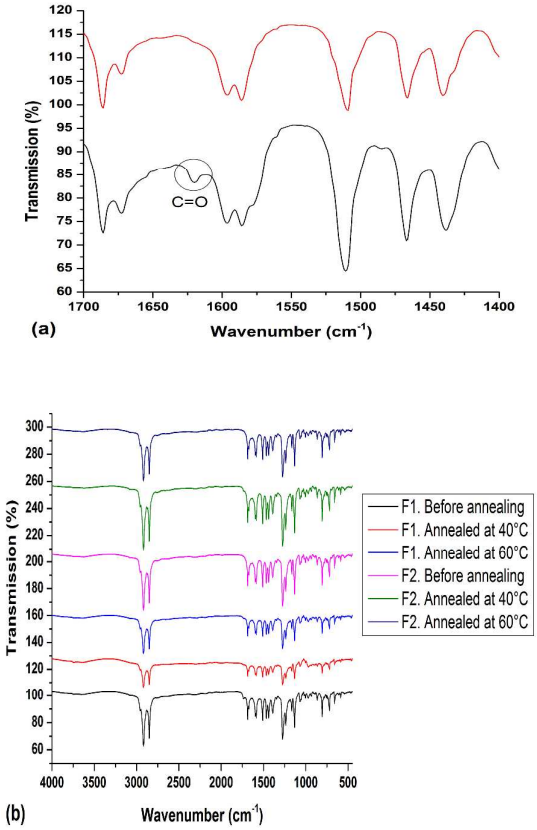

Fig. 5 FTIR spectra of: (a) **1** (black) and F1 annealing (red); and (b) F1 and F2 before and after annealing at 40 °C and 60 °C.

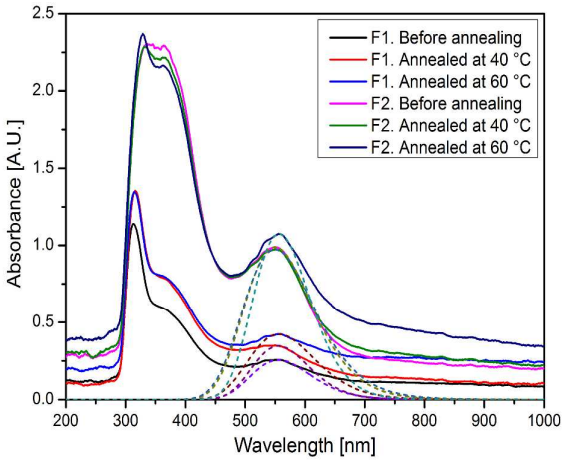

Fig. 6 UV-vis spectra of F1 and F2 (the deconvoluted spectra are shown by dashed lines).

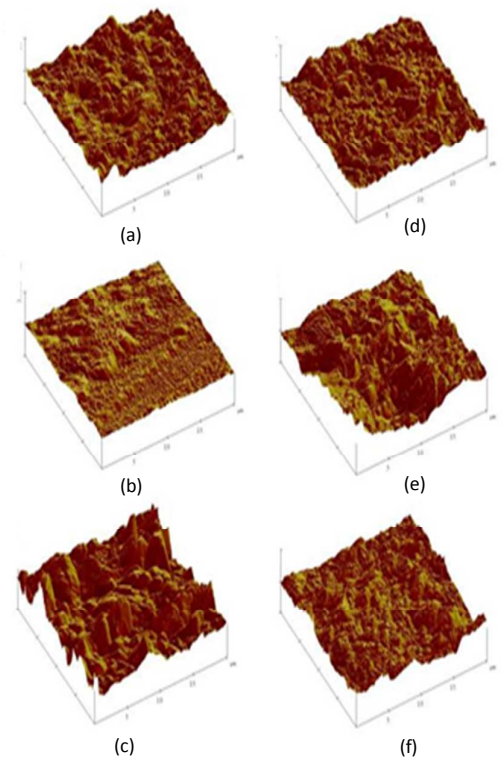

Fig. 7 AFM of F1: (a) before annealing, (b) annealed at 40 °C, and (c) annealed at 60 °C; and F2 (d) before annealing, (e) annealed at 40 °C, and (f) annealed at 60 °C.

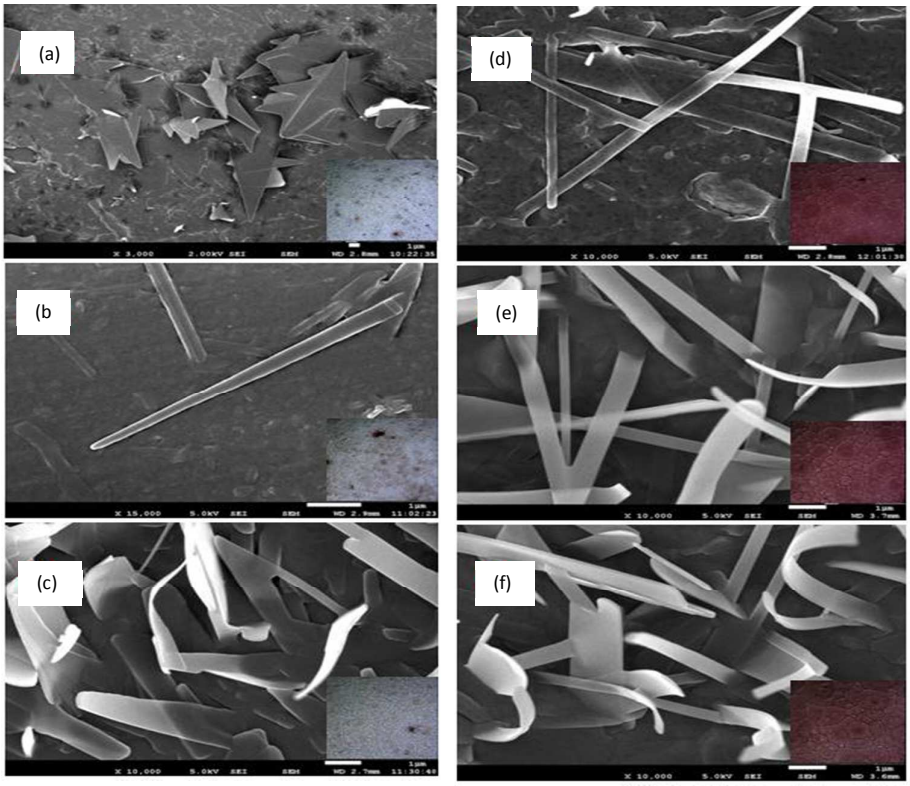

Fig. 8 FESEM images of: F1 (3000x) before annealing (a), annealed at 40 °C (b), and annealed at 60 °C (c); F2 before annealing (d), annealed at 40 °C (e), and annealed at 60 °C (f).

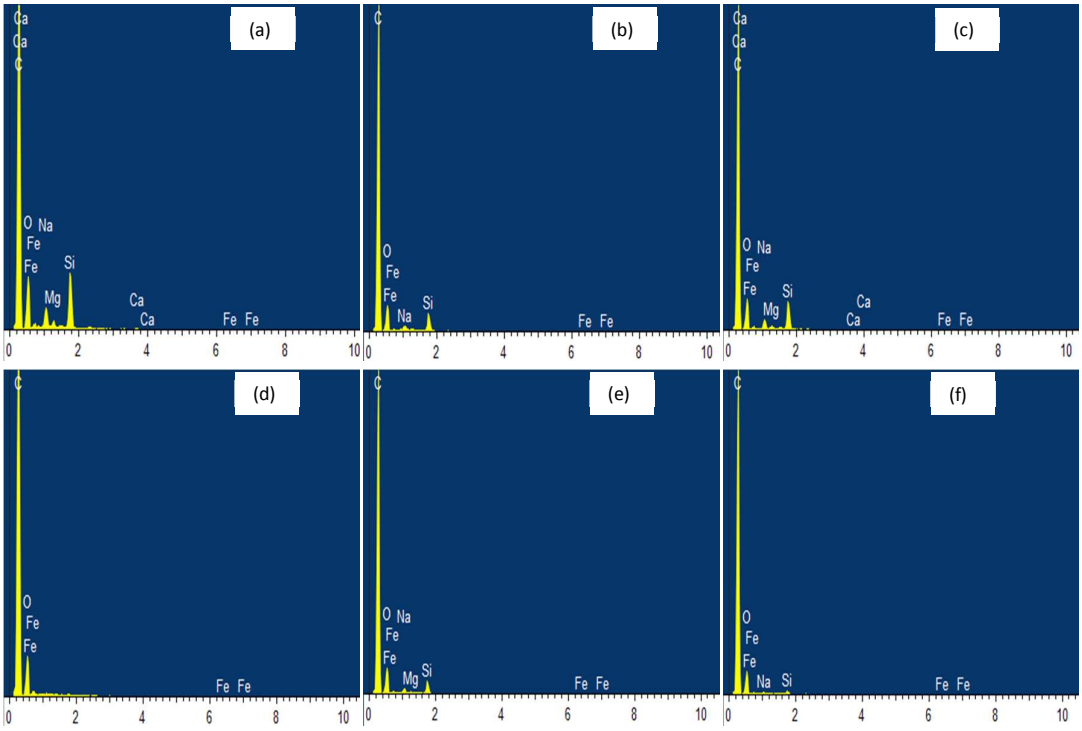

Fig. 9 EDX analyses for the surface of F1 before annealing (a), annealed at 40 °C (b), and annealed at 60 °C (c), and F2 before annealing (d), annealed at 40 °C (e), and annealed at 40 °C (f).